Research Article | Open Access

Greenverse Science

Yin *et al. Greenverse Sci.* **2026**, *1*, 10 **DOI:**10.20517/greenvsci.2026.07

Amine-mediated, oxygen-tolerant concerted capture and electrochemical conversion of CO_2 from flue gas

Chun-Qing Yin, Ye-Bin Zou, Zhi-Hui Lv, Lin Du, Yan Li*, Xin-Ming Hu*

Keywords:
CO_2 capture, CO_2 conversion, electrocatalysis, concerted system, oxygen tolerance

Citation: Yin, C. Q.; Zou, Y. B.; Lv, Z. H.; Du, L.; Li, Y.; Hu, X. M. Amine-mediated, oxygen-tolerant concerted capture and electrochemical conversion of CO_2 from flue gas. *Greenverse Sci.* **2026**, *1*, 10. https://dx.doi.org/10.20517/greenvsci.2026.07

Received: 17 Mar 2026
First Decision: 13 Apr 2026
Revised: 10 May 2026
Accepted: 1 Jun 2026
Published: 23 Jun 2026

Academic Editor: Dengsong Zhang
Copy Editor: Xing-Yue Zhang
Production Editor: Xing-Yue Zhang

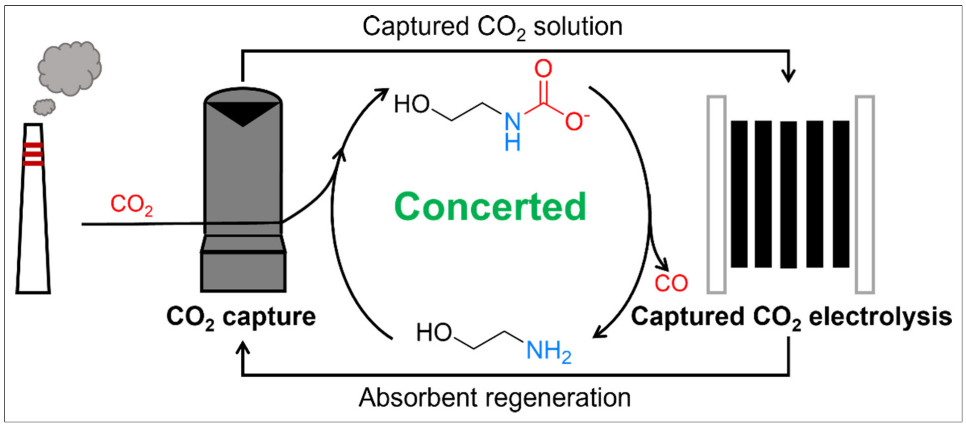

Abstract

Integrated capture and electrochemical conversion of CO_2 from flue gas can mitigate the energy penalties of conventional decoupled processes, offering a promising pathway to reduce CO_2 emissions and valorize carbon resources. However, this strategy has not yet been fully realized because of the mismatch between the rates of CO_2 capture and electrolysis. Herein, we report a concerted system integrating CO_2 capture and electrochemical conversion from flue gas using monoethanolamine (MEA) as the mediator. MEA captures CO_2 from flue gas and delivers it in liquid form to an electrolyzer, where the captured CO_2 is electrochemically converted into CO with concurrent MEA regeneration. The regenerated MEA is recycled to the absorber for another round of CO_2 capture, establishing a sustainable closed loop for simultaneous CO_2 capture and electrolysis. Owing to the low solubility of O_2 in the MEA solution, the system exhibits strong oxygen tolerance, avoiding efficiency loss caused by the competing oxygen reduction reaction. By examining key parameters such as current density, electrode hydrophobicity, and CO_2 concentration, the concerted system achieves a high CO_2 capture efficiency of 63% for flue gas containing 15% CO_2 and produces a syngas with an H_2/CO = 3.2 over 24 h of operation. This work demonstrates the first MEA-based system for concerted capture and conversion of CO_2 from flue gas, offering an effective strategy for sustainable carbon recycling and syngas production.

Environment Research Institute, Shandong University, Qingdao 266237, Shandong, China.

*Correspondence to: Dr. Yan Li, Prof. Xin-Ming Hu, Environment Research Institute, Shandong University, Qingdao 266237, Shandong, China. E-mail: liyan2024@sdu.edu.cn; huxm@sdu.edu.cn

INTRODUCTION

The continuous rise in atmospheric CO_2 concentrations has led to severe environmental issues, including global warming, ocean acidification, and biodiversity loss[1,2]. Carbon capture and utilization (CCU) technologies have garnered increasing attention due to their capability of reducing CO_2 emissions while simultaneously producing value-added chemicals and fuels[3-5]. For example, porous materials have been widely studied for CO_2 capture and catalytic conversion, due to their high surface area and tunable structures[6-8]. Among CCU technologies, electrochemical CO_2 reduction reaction (CO_2RR) is particularly promising, because it can use renewable electricity (e.g., wind and solar power) to convert CO_2 under mild conditions into a variety of valuable products such as CO and formic acid[9,10]. Currently, most studies on CO_2RR are performed using high-purity CO_2 gas in lab-scale electrolyzers. In practice, industrial flue gas, the main point source of anthropogenic CO_2 emissions, contains 5%-15% CO_2 mixed with N_2, O_2, and other gas impurities. Direct electrolysis of flue gas in gas-fed electrolyzers is challenging because the presence of O_2 severely hinders CO_2RR by triggering the thermodynamically more favorable oxygen reduction reaction (ORR), resulting in reduced selectivity and increased energy loss [Figure 1, Path I][11,12]. Moreover, the low CO_2 concentration in the flue gas leads to low reaction efficiency[13,14].

To overcome these issues, a sequential approach for CO_2 capture and conversion from flue gas has been widely adopted [Figure 1, Path II][15-17]. In this process, CO_2 is first absorbed from flue gas using alkaline absorbents such as KOH or amine solutions, forming captured CO_2 solutions enriched with (bi)carbonates or carbamates. This is usually followed by thermal treatment to release CO_2 while simultaneously regenerating the absorbent. The purified CO_2 is compressed and transported for subsequent conversion in a gas-fed electrolyzer[18]. Although effective at separating CO_2 from flue gas and converting it, this approach involves high energy consumption and capital investment, limiting its economic viability[19,20]. For instance, capturing CO_2 using a commercial absorbent such as monoethanolamine (MEA) requires up to 4.3 GJ/tCO_2 for MEA regeneration[21]. Additionally, solvent degradation and equipment corrosion are more likely to occur at elevated temperatures, thereby increasing operational complexity[22,23].

Electrochemical conversion of captured CO_2 solution has recently emerged as a promising alternative to the conventional sequential CO_2 capture and conversion approach, offering the potential to simplify the overall process and reduce energy consumption [Figure 1, Path III][24]. In this strategy, CO_2 capture and conversion occur alternately: CO_2 is captured by alkaline absorbents such as carbonates or MEA to form a captured CO_2 solution, which is then fed into an electrolyzer where CO or other products are electrochemically produced. After the reaction, the regenerated alkaline absorbent can be reused for another round of CO_2 capture and conversion. For instance, Zhang *et al.* reported the direct electrolysis of captured CO_2 solution (i.e., bicarbonate, obtained by capturing CO_2 in a carbonate solution) in a membrane electrode assembly with a silver foam cathode, achieving a Faraday efficiency for CO (FE_{CO}) of 60%[25]. Later, Song *et al.* developed a Ni-based single-atom catalyst (Ni-SAC) for electrolysis of $KHCO_3$ solution, achieving a much higher FE_{CO} exceeding 90%[26]. In comparison, Leverick *et al.* attained a relatively low FE_{CO} of ~19% when employing a simple Ag foil electrode to electrolyze a CO_2-capturing MEA solution[27].

While path III effectively integrates CO_2 capture and conversion, it relies on pre-captured CO_2. During extended electrolysis, the consumption of captured CO_2 without replenishment decreases its concentration, leading to a drop in product selectivity[28]. This limitation highlights the need for a concerted CO_2 capture and conversion system operating simultaneously. However, such a strategy has not yet been realized due to the inherent mismatch between the rates of CO_2 capture and electrolysis. This raises a critical question: can the electrolytically regenerated absorbent maintain adequate alkalinity to capture CO_2 effectively and sustain the supply of captured CO_2 species for subsequent conversion cycles at comparable rates[29,30]? Recent work has demonstrated a coupled system comprising a K_2CO_3 absorption column and an electrolyzer, which achieved a CO_2

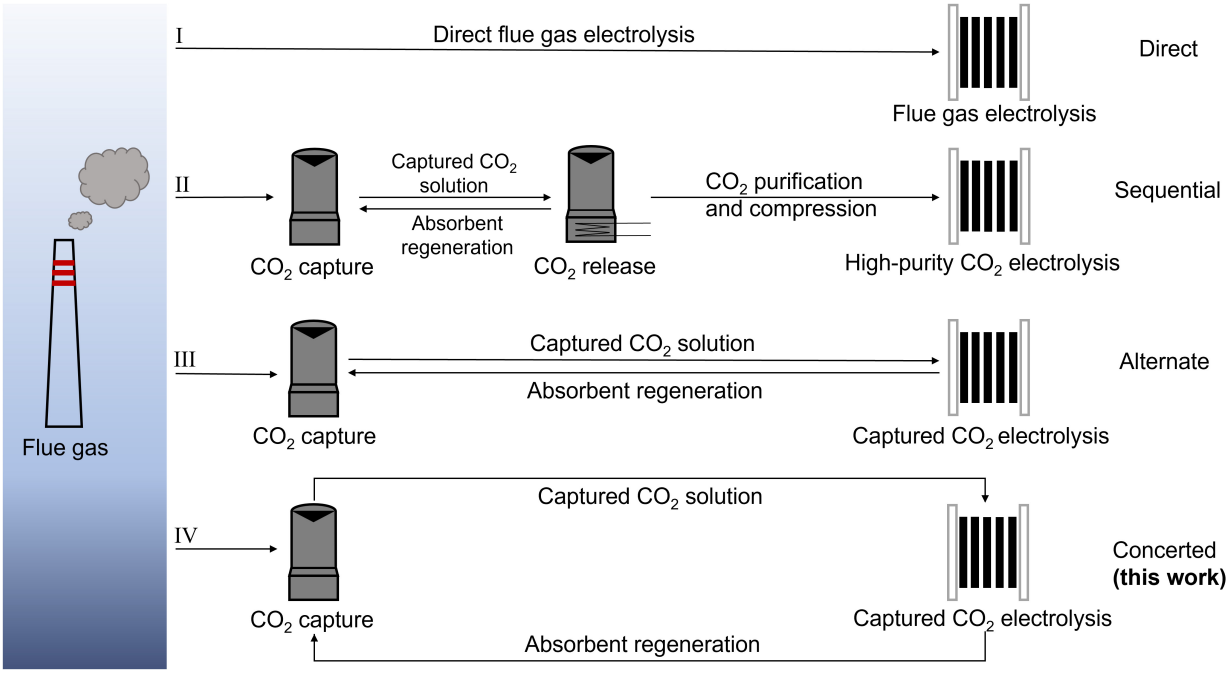

Figure 1. Schematic illustration of various pathways for CO_2 valorization from industrial flue gas. Path I represents the direct flue-gas electrolysis in gas-fed electrolyzers without capture steps. Path II illustrates a sequential route for CO_2 capture and electrolysis, with electrolysis also carried out in a gas-fed electrolyzer. Path III depicts the alternate route in which captured CO_2 is directly converted via electrolysis of the captured CO_2 solution, while the regenerated absorbent is reused for subsequent CO_2 capture. Path IV shows the concerted route for simultaneous CO_2 capture and electrolysis reported in this work.

capture efficiency of 30% and an FE_{CO} of 35%, validating the feasibility of such a concerted approach[31]. Nonetheless, carbonate-based absorbent solutions suffer from slow CO_2 absorption kinetics, hindering their practical applications[32]. In comparison, MEA exhibits faster reaction kinetics and higher industrial maturity for CO_2 capture, making it a more promising candidate for practical deployment[33,34].

Herein, we report an MEA-based concerted CO_2 capture-conversion system by coupling a CO_2 absorber with a liquid-fed electrolyzer for continuous syngas production from simulated flue gas (containing 15% CO_2, 5% O_2, and 80% N_2) [Figure 1, Path IV]. A bipolar membrane (BPM) is utilized to generate protons, which react with the carbamate/bicarbonate species formed during CO_2 capture in MEA, enabling *in situ* CO_2 liberation for subsequent electrochemical reduction to CO. Meanwhile, MEA is regenerated and recycled back to capture additional CO_2, forming a concerted system for simultaneous CO_2 capture and electrochemical conversion. During electrolysis, H_2 is also produced from the reduction of protonated MEA generated during CO_2 capture, forming a syngas with H_2/CO = 3.2. *In situ* electrochemical spectroscopy is performed to elucidate the reaction processes occurring at the electrode surface.

EXPERIMENTAL

Chemicals and materials

Chemicals

Nickel chloride hexahydrate ($NiCl_2 \cdot 6H_2O$), melamine ($C_3H_6N_6$), potassium hydroxide (KOH), polytetrafluoroethylene suspension (PTFE, 60 wt%), and MEA were purchased from Shanghai Aladdin Bio-Chem Technology Co., Ltd. Lithium chloride (LiCl) and potassium chloride (KCl) were obtained from Shanghai Maclin Biochemical Technology Co., Ltd. Nafion solution (5 wt%) was purchased from Sigma-Aldrich Chemical Reagent Co., Ltd. Methanol, ethanol, and isopropanol were acquired from Sinopharm Chemical Reagent Co., Ltd. Polyethylene terephthalate (PET) plastic waste was acquired from used Nongfu Spring mineral water bottles. All reagents used in this work were obtained from commercial suppliers and used without further purification.

Catalyst synthesis

The catalyst was synthesized according to a reported procedure[35]. A homogeneous mixture was prepared by grinding 1.0 g of $NiCl_2·6H_2O$, 2.0 g of melamine, 5.5 g of KCl, and 4.5 g of LiCl in a mortar. Next, 2.0 g of PET plastic (obtained from used mineral water bottles) was cut into small pieces (~0.5 × 0.5 cm^2) and added to the mixture. The resulting mixture was transferred to a quartz boat and pyrolyzed in a tube furnace at 800 °C for 2 h under an Ar atmosphere. After cooling to room temperature, the product was washed with 80 mL of 1.0 M HCl at 60 °C, then rinsed with ultrapure water and methanol, and dried overnight at 60 °C. Finally, a secondary carbonization step was performed under the same pyrolysis conditions, yielding the target atomic nickel and nitrogen-doped carbon (Ni-N-C) material. The Ni content in the material was determined to be 2.54 wt% by inductively coupled plasma optical emission spectroscopy, as reported previously.

Electrochemical measurements

Electrolysis of simulated flue gas

The working electrode was prepared as follows: 16 mg of catalyst, 400 μL of 5% PTFE suspension, 3.6 mL of isopropanol, and 16 μL of 5 wt% Nafion were mixed and sonicated for 30 min to obtain a uniform catalyst ink. The resulting dispersion was then drop-cast onto the gas-diffusion layer (GDL) side of a carbon paper, which was placed on a 40 °C heating plate to facilitate solvent evaporation. After drying, a gas diffusion electrode with an effective area of 1 cm^2 (matching the serpentine channel of the membrane electrode assembly) was obtained, with a catalyst loading of 1 $mg·cm^{-2}$. Electrolysis was performed in a membrane electrode assembly electrolyzer on an electrochemical workstation (Gamry Interface 1010E, USA). The working and counter (IrO_x/Ti mesh) electrodes were placed on opposite sides of an anion exchange membrane (AEM, Fumasep FAA-3-PE-30). 1.0 M KOH was used as the anodic electrolyte and circulated through the anodic compartment via a peristaltic pump. A flow of simulated flue gas (15% CO_2/85% N_2 or 15% CO_2/80% N_2/5% O_2) was directly fed into the cathodic compartment at a rate of 20 sccm. The gaseous products after 15 min of electrolysis were directly analyzed by a gas chromatograph (Fuli GC9790II, China).

Electrolysis of the CO_2-capturing MEA solution

The working electrodes were prepared as follows: a mixture of 16 mg of the catalyst, 16 μL of Nafion solution (5 wt%), and 3.6 mL of isopropanol was sonicated for 30 min. The resulting suspension was drop-cast onto a hydrophilic carbon paper (TGP-H-060) with an effective area of 1 cm^2, achieving a catalyst loading of 4 $mg·cm^{-2}$. A titanium mesh plated with iridium oxide (IrO_x/Ti) served as the counter electrode. Electrolysis was performed in the same membrane electrode assembly electrolyzer using the same electrochemical workstation (Gamry Interface 1010E) as for the electrolysis of flue gas. The working and counter electrodes were placed on opposite sides of a BPM (FBM-PK). The anodic compartment was filled with 70 mL of 1.0 M KOH, which was continuously circulated by a peristaltic pump at a rate of 50 mL/min. The cathodic compartment contained 70 mL of a CO_2-capturing MEA solution (100% CO_2 gas was used for CO_2 capture) and was circulated at 100 mL/min. During the experiment, CO_2, N_2, O_2, or simulated flue gas with varying O_2 concentrations was continuously sparged into the cathodic electrolyte at a constant flow rate of 20 sccm, controlled by a gas flowmeter. The dissolved oxygen concentration was measured using a dissolved oxygen meter (INESA Scientific Instrument Co., Ltd., JPBJ-610L, China). The gaseous products were analyzed after 15 min of electrolysis using in-line gas chromatography, while the cathodic electrolyte was characterized by nuclear magnetic resonance (NMR) spectroscopy.

Concerted CO_2 capture and electrolysis

Before initiating the concerted capture and electrolysis process, simulated flue gas (15% CO_2/5% O_2/80% N_2 or 5% CO_2/5% O_2/90% N_2) was introduced at a flow rate of 50 sccm into an MEA solution for CO_2 capture. The pH of the solution was monitored using a pH meter (Hangzhou Meiyi, SUP-PH6.5-5022-YK-IFS15, China). When the CO_2 capture was completed, electrolysis was initiated, and CO_2 capture and electrolysis were carried out simultaneously under continuous flue gas feeding at a flow rate of 5 sccm. The CO_2-capturing MEA solution was transported through pipelines to the cathodic compartment of the membrane electrode assembly for electrolysis, while the regenerated MEA solution was recycled back to the capture unit through a peri-

staltic pump to capture CO_2 again. Electrolysis in the concerted system was carried out using a membrane electrode assembly with an effective area of 4 cm^2. Two types of working electrodes were prepared to investigate the effect of electrode hydrophobicity on electrolysis efficiency by incorporating the hydrophobic polymer PTFE. For the PTFE-free electrode (Ni-N-C), the catalyst ink was prepared by mixing 16 mg of catalyst, 16 μL of Nafion solution (5 wt%), and 3.6 mL of isopropanol. For the PTFE-containing electrode (Ni-N-C-PTFE), 100 μL of 2 wt% PTFE dispersion was added to the same mixture. Each mixture was ultrasonicated for 30 min, and the resulting suspension was drop-cast onto a hydrophilic carbon paper (TGP-H-060). The final electrode had an effective area of 4 cm^2 and a catalyst loading of 4 $mg \cdot cm^{-2}$. The gas outlet of the cathodic chamber was connected to gas chromatography for real-time analysis of gaseous products, while the cathodic electrolyte was characterized by NMR spectroscopy. The data were analyzed using Microsoft Excel (Version 2021), and the average of two replicate measurements is reported where applicable.

The Faraday efficiencies (FE) of CO and H_2 were calculated using Equation 1.

$$FE = \frac{n \times f \times v \times F \times P}{I \times R \times T} \times 100\% \quad (1)$$

where n is the number of electrons transferred for the formation of a specific product (2 for both CO or H_2); f is the volume concentration of CO or H_2 in the gas flow; v is the gas flow rate; F is the Faraday constant, 96,485 $C \cdot mol^{-1}$; P is the atmospheric pressure, 101,325 Pa; I is the current at the given sampling time; R is the ideal gas constant, 8.314 $J \cdot mol^{-1} \cdot K^{-1}$; T is room temperature.

The capture efficiency of CO_2 was calculated according to Equation 2.

$$CO_2 \text{ capture efficiency} = \frac{A - A_t}{A} \times 100\% \quad (2)$$

where A is the chromatographic peak area of CO_2 leaving the concerted system without electrolysis; A_t is the peak area of CO_2 leaving the concerted system after a certain electrolysis time (t).

During the prolonged electrolysis, the gaseous products were analyzed at 0.5-h intervals using gas chromatography. The volume concentrations (f_t) of CO and H_2 at each time point (t) were determined based on calibration curves. Accordingly, the volumes of CO and H_2 produced during the first 0.5 h of electrolysis ($V_{0\sim0.5}$) were calculated according to Equation 3.

$$V_{0\sim0.5} = f_{0.5} \times v \times 0.5 \quad (3)$$

Gas chromatographic analysis indicated that the volume concentrations of CO and H_2 changed over time, as shown by the decrease in FE_{CO} and a corresponding increase in FE_{H_2}. Consequently, for electrolysis conducted beyond 0.5 h, the average volume concentration of CO or H_2 over each 0.5-hour interval was employed to calculate the gas volumes produced during that period ($V_{t-0.5\sim t}$) according to Equation 4.

$$V_{t-0.5\sim t} = \frac{f_{t-0.5} + f_t}{2} \times v \times t \quad (4)$$

The total volumes of CO and H_2 produced during electrolysis over a specific time (t) were determined according to Equation 5.

$$V_t = V_{0\sim0.5} + V_{0.5\sim1} + \ldots + V_{t-0.5\sim t} \quad (5)$$

NMR measurement

^1H and ^{13}C NMR spectra were recorded on a Bruker AVANCE NEO spectrometer (Germany) operating at a resonance frequency of 600 MHz. For sample preparation, 500 μL of the solution was mixed with 140 μL of 5 mM dimethyl sulfoxide (in D_2O/H_2O, $V_{D_2O}/V_{H_2O} = 19/1$). The mixture was then transferred to a tube for ^1H and ^{13}C NMR analysis. The ^1H NMR spectra were recorded in water-suppressed mode.

In situ attenuated total reflection Fourier transform infrared measurement

In situ attenuated total reflection Fourier transform infrared (ATR-FTIR) spectra were obtained using a Bruker INVENIO infrared spectrometer (Germany) equipped with a mercury cadmium telluride detector. The working electrode was prepared by depositing the Ni-N-C catalyst ink (same as used previously) onto a gold-coated silicon prism. The Ag/AgCl and platinum wire were used as reference and counter electrodes, respectively. The electrolyte

was prepared by saturating a 2 M MEA solution with a simulated flue gas composed of 15% CO_2/5% O_2/80% N_2. During electrolysis, 5 sccm of N_2 was continuously purged into the electrolyte solution. The IR spectra were recorded during electrolysis at potentials ranging from -0.6 to -1.7 V *vs.* Ag/AgCl in 0.1 V intervals. Each spectrum was collected over 100 scans at a resolution of 4 cm^{-1}. The background spectrum was recorded at -0.6 V *vs.* Ag/AgCl for baseline subtraction.

RESULTS AND DISCUSSION

Catalysts are essential for converting CO_2 into valuable products, such as CO, an important feedstock for the chemical industry. Three main types of catalysts have been reported for CO_2-to-CO conversion, including noble metal catalysts (e.g., Au and Ag)[36-38], molecular metal complex catalysts (e.g., cobalt phthalocyanine supported on carbon black, CoPc/CB)[39,40], and metal-nitrogen-carbon (M-N-C) catalysts[41,42]. Noble metal catalysts exhibit high activity but are costly, limiting their practical applications. Molecular catalysts such as CoPc/CB can offer good selectivity but often suffer from limited stability under continuous electrolysis conditions[28]. In contrast, M-N-C catalysts feature abundant active sites, high activity, and structural robustness, making them promising candidates for CO_2 electroreduction[43]. In particular, Ni-N-C catalysts with well-defined active Ni-N sites have shown high activity and selectivity for CO_2-to-CO conversion[44-46]. Therefore, a Ni-N-C single-atom catalyst is used as a model catalyst in this study because of its established CO selectivity and well-understood active site structure. The Ni-N-C is prepared according to previously reported procedures[35].

A liquid-fed electrolyzer is first fabricated for the electrochemical conversion of CO_2 captured in an MEA solution [Supplementary Figure 1]. The electrolyzer comprises an IrO_x/Ti mesh anode and a carbon paper cathode coated with a Ni-N-C catalyst. Both electrodes are firmly pressed between serpentine flow plates on the anodic and cathodic sides. The active area of the electrode is 1 cm^2. A 1 M KOH solution is used as the anolyte. A CO_2-capturing 5 M MEA solution, prepared by bubbling CO_2 into the MEA solution until CO_2 capture is completed, is used as the catholyte. NMR spectroscopy shows that the CO_2-capturing 5 M MEA solution primarily contains ammonium, carbamate, and bicarbonate [Supplementary Figure 2].

A BPM is inserted between the anode and cathode to physically separate the two compartments. Under reverse-bias operation, the BPM promotes water dissociation, supplying hydroxide anions (OH^-) to the anode and protons (H^+) to the cathode. At the anode, OH^- is oxidized at the IrO_x/Ti mesh surface to produce O_2 and H_2O. At the cathode, H^+ can react with carbamate and bicarbonate species in the CO_2-capturing MEA solution to liberate *in situ* CO_2, which is then reduced at the Ni-N-C catalyst. Electrochemical performance is evaluated at constant current densities of 50, 100, and 200 $mA{\cdot}cm^{-2}$, with N_2, CO_2, or simulated flue gas continuously sparged into the electrolyte. Gaseous products generated after electrolysis are analyzed using online gas chromatography, confirming that only CO and H_2 are produced. ^{1}H NMR analysis does not show detectable products in the electrolyte.

Following the construction of the liquid-fed electrolyzer, we first evaluate the effect of the gas atmosphere on the electrochemical conversion efficiency of the CO_2-capturing MEA solutions. Under continuous pure CO_2 sparging, the FE_{CO} is 34%, 32%, and 15% at 50, 100, and 200 $mA{\cdot}cm^{-2}$, respectively, with the remaining FE attributed to the hydrogen evolution reaction (HER) [Supplementary Figure 3A]. When the atmosphere is switched to 15% CO_2/85% N_2 or pure N_2, comparable FE_{CO} and cell voltages are observed [Supplementary Figure 3]. This result indicates that even under limited or no CO_2 feed, the chemically captured CO_2 in MEA solution can be effectively utilized for electrochemical CO production.

The conversion efficiencies of CO_2-capturing MEA using a BPM and an AEM are also compared. Because no H^+ is produced at the AEM and no CO_2 is liberated, replacing the BPM with an AEM leads to a decrease in CO production, despite the lower cell voltage with an AEM [Supplementary Figure 4]. This result further confirms the critical role of H^+ generated at the BPM in reacting with carbamate/bicarbonate to liberate *in situ* CO_2, which is essential for subsequent conversion to produce CO.

Given that practical CO_2 sources often contain high concentrations of O_2 ranging from 2% to 12%[47], the effect of O_2 on the electrochemical conversion of CO_2-capturing MEA is investigated under simulated flue gas conditions, with the CO_2 concentration fixed at 15% and the O_2 adjusted using N_2. For comparison, a gas-fed electrolyzer, structurally identical to the liquid-fed system except for the use of an AEM and the addition of a microporous layer on the carbon paper cathode, is also examined [Supplementary Figure 5]. In the gas-fed electrolyzer, the linear sweep voltammetry shows that the onset potential for reduction current shifts positively upon the introduction of 5% O_2 into the CO_2/N_2 stream (15% CO_2/80% N_2/5% O_2), indicating substantial activity of Ni-N-C for O_2 reduction [Supplementary Figure 6]. Moreover, neither CO nor H_2 product is detected during the electrolysis of 15% CO_2/80% N_2/5% O_2 at current densities of 50 and 100 mA·cm^{-2}, in stark contrast to the electrolysis of 15% CO_2/85% N_2 (FE_{CO} = 81% at 50 mA·cm^{-2} and 63% at 100 mA·cm^{-2}), suggesting nearly all electrons are diverted to the competing ORR when 5% O_2 is present in the gas-fed electrolyzer [Figure 2A and Supplementary Figure 7]. Correspondingly, the cell voltages recorded in the presence of O_2 are lower than those recorded under O_2-free conditions. At an increased current density of 200 mA·cm^{-2}, 45% FE_{H_2} and 1% FE_{CO} are detected, though ORR remains the dominant reaction.

In contrast, the cell voltage for the reduction current observed in CO_2-capturing MEA solution under a gas mixture of 15% CO_2/80% N_2/5% O_2 is quite similar to that under 15% CO_2/85% N_2 [Supplementary Figure 8]. The FE_{CO} is 31%, 29%, and 16% at 50, 100, and 200 mA·cm^{-2}, respectively, which are similar to those recorded under O_2-free conditions [Figure 2B and Supplementary Figure 9]. Notably, no obvious decrease in FE_{CO} is observed when the O_2 concentration increases to 10%, 20%, or even 100% [Supplementary Figure 10]. To further quantify the oxygen effect, the dissolved oxygen concentration in the electrolyte is measured under 15% CO_2/85% N_2, 15% CO_2/80% N_2/5% O_2, and 100% O_2 conditions, with each gas continuously bubbled into the solution for 30 min [Supplementary Figure 11]. The dissolved oxygen concentration is 0.003 mM under 15% CO_2/85% N_2, 0.060 mM under 15% CO_2/80% N_2/5% O_2, and 0.492 mM under 100% O_2 after 30 min. Despite the large differences in dissolved oxygen concentration, the FE_{CO} in the liquid-fed system remains comparable across all tested conditions. This indicates that O_2 in the flue gas stream has negligible influence on the electrochemical conversion of CO_2-capturing MEA solution, making the system oxygen-tolerant.

Figure 2C illustrates the electrolysis process in the gas-fed and liquid-fed electrolyzers in the presence of O_2. In the gas-fed electrolyzer, the ORR dominates over CO_2 reduction due to its more favorable thermodynamics and comparable concentrations to CO_2, thereby suppressing CO production, which aligns with previous studies[48,49]. However, the impact of O_2 is negligible in the liquid-fed electrolyzer. In aqueous media, the solubility of O_2 is only 0.0012 M (1 atm, 298 K), much lower than that of CO_2 (0.034 M, 1 atm, 298 K)[50,51]. The inherently low O_2 solubility limits its concentration at the cathode, allowing CO_2 electroreduction to proceed without complications arising from O_2 reduction, regardless of the O_2 concentrations in the gas phase. Additionally, H^+ generated by the BPM reacts with carbamate/bicarbonate species to release CO_2 *in situ*, ensuring a high local CO_2 concentration at the electrode surface for electroreduction. These results highlight the large potential of the concerted pathway for capture and conversion of CO_2 from flue gas.

After validating the direct conversion of CO_2-capturing MEA solution, we establish a concerted CO_2 capture and conversion system by coupling a simple CO_2 absorber with an electrolyzer designed for CO_2-capturing MEA [Figure 3A]. To enhance both CO_2 capture efficiency and CO production rate, the active area of the Ni-N-C electrode is increased to 4 cm^2. A 2 M MEA solution is selected as the capture medium because it provides an optimal trade-off, achieving a higher FE_{CO} than 1 M MEA and a comparable FE_{CO} to 5 M MEA while operating at a lower cell voltage [Supplementary Figure 12]. The capture of CO_2 from simulated flue gas (15% CO_2/80% N_2/5% O_2) is performed by continuously bubbling the flue gas into the MEA solution at

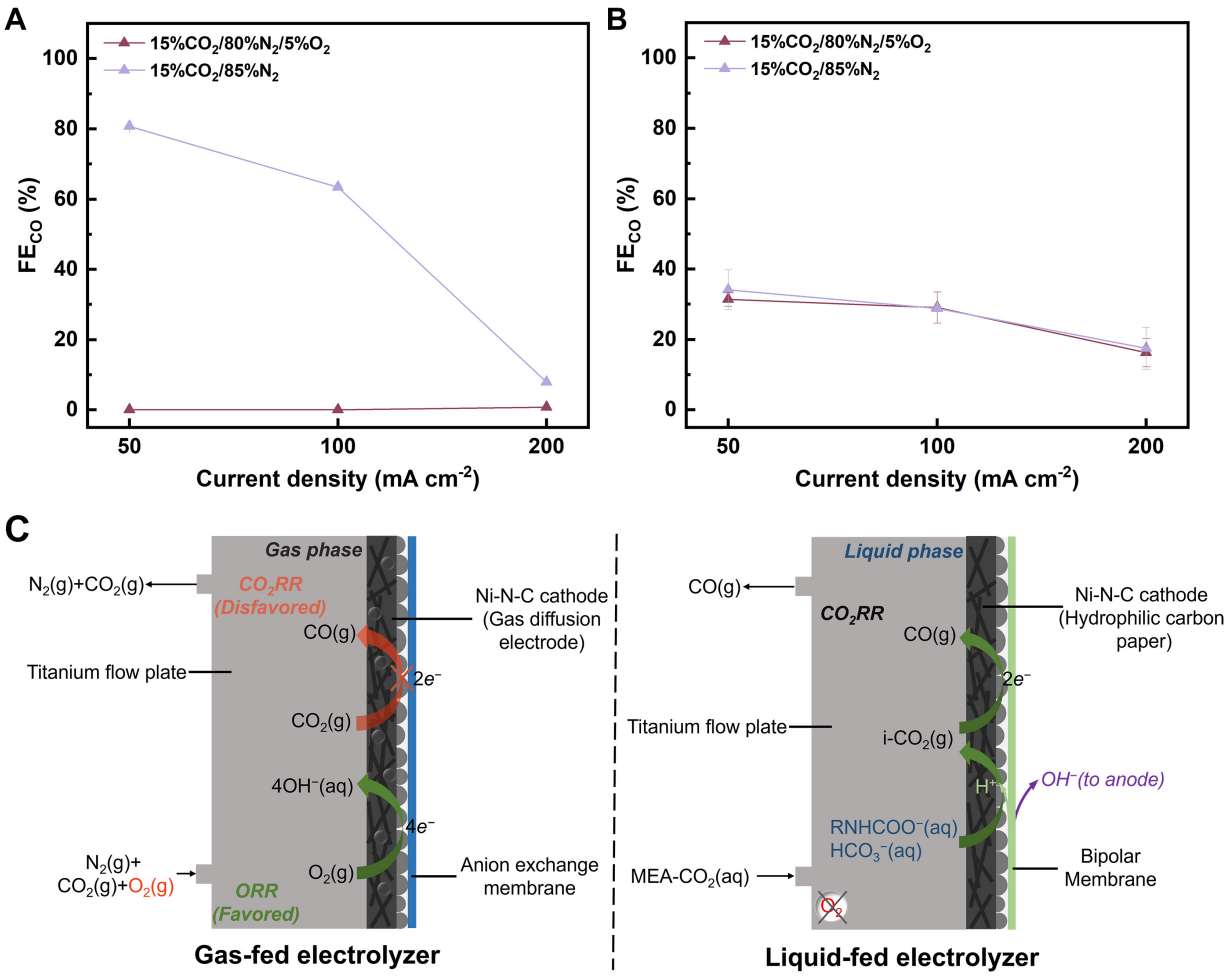

Figure 2. FE_{CO} recorded for electrolysis of (A) 15% CO_2/80% N_2/5% O_2 and 15% CO_2/85% N_2 in the gas-fed electrolyzer and (B) CO_2-capturing 5 M MEA under 15% CO_2/80% N_2/5% O_2 and 15% CO_2/85% N_2 atmosphere in the liquid-fed electrolyzer. The error bars represent the standard deviation of two independent measurements; (C) Schematic diagrams of reaction processes in the cathodic chambers of the gas-fed and liquid-fed electrolyzers. FE: Faraday efficiencies; FE_{CO}: Faraday efficiency for CO; MEA: monoethanolamine; CO_2RR: CO_2 reduction reaction; ORR: oxygen reduction reaction.

50 sccm for 12 h. The completion of CO_2 capture is confirmed when the outlet CO_2 concentration approaches the inlet level (~15%), and the pH decreases from 12.0 to 8.3 [Figure 3B]. The final pH is slightly higher than that for capture of pure CO_2 (pH 7.7), which is consistent with Henry's Law because of the lower partial pressure of CO_2 in flue gas. The CO_2-capturing MEA solution is subsequently electrolyzed at a constant current density of 50 mA·cm^{-2}, with a flue gas flow rate of 5 sccm and a solution flow of 200 mL/min. Meanwhile, the regenerated MEA solution is circulated throughout the system, enabling concerted capture and electrochemical conversion of CO_2.

The system achieves a maximum FE_{CO} of 26% after 2 h of operation at 50 mA·cm^{-2} [Figure 3C]. The FE_{CO} then gradually declines to 14% over the next 22 h of operation, with a cumulative production of 401 mL CO and 1,531 mL H_2, forming a syngas with H_2/CO = 3.8 [Figure 3D]. Meanwhile, the concentration of CO_2 in the flue gas after CO_2 capture ($[CO_2]_{outlet}$) decreases markedly during the first 12 h and changes only slightly thereafter [Figure 3B]. Correspondingly, the CO_2 capture efficiency increases during the first 12 h, then becomes relatively stable over the subsequent 12 h, and ultimately reaches a maximum of 64% [Figure 3E]. These observations indicate that MEA is gradually regenerated as the 15% CO_2-capturing MEA solution is electrochemically converted, enabling the solution to capture increasing amounts of CO_2 from the flue gas. After

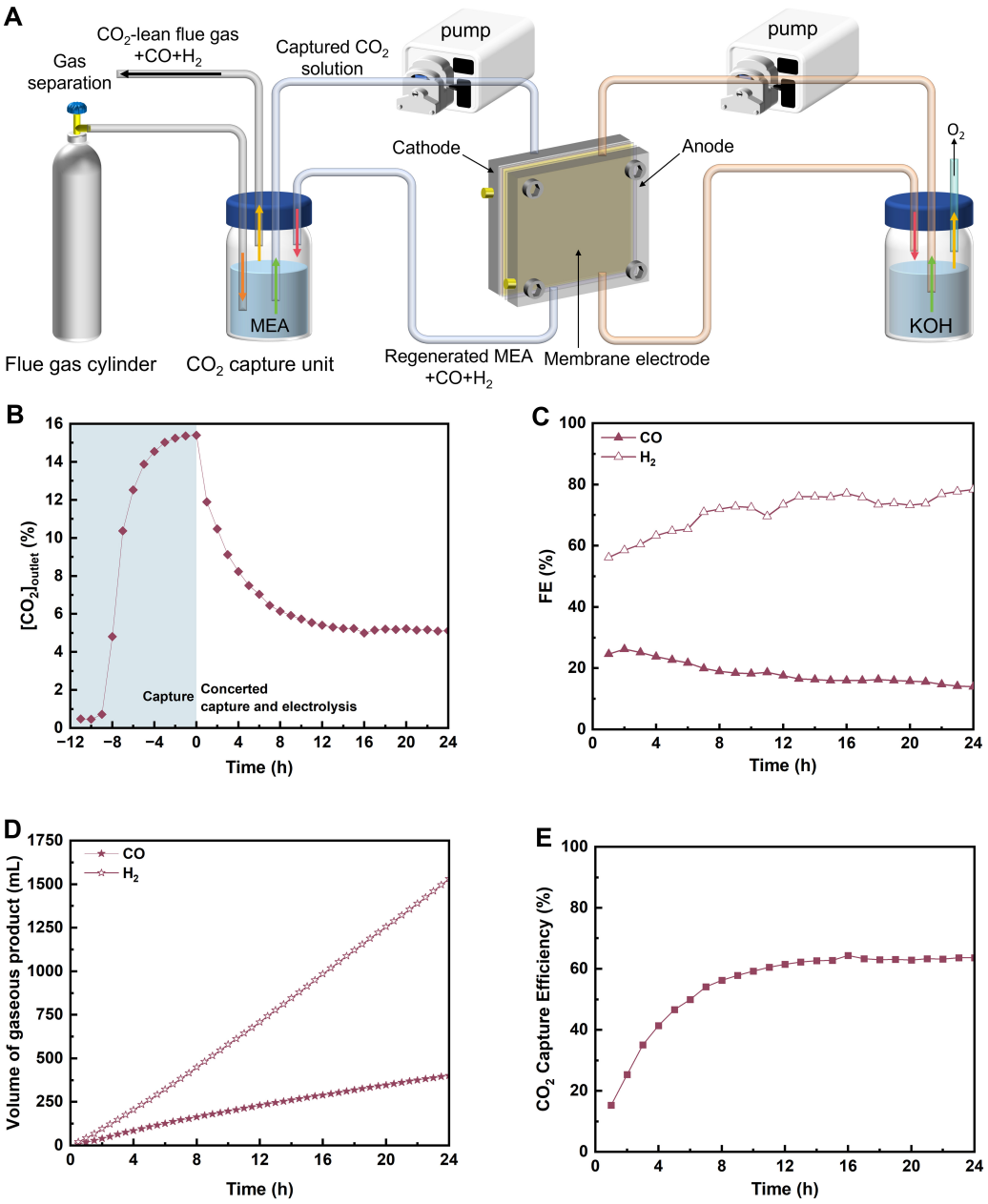

Figure 3. (A) Schematic illustration of a concerted CO_2 capture and conversion system; (B-E) Efficiency of the concerted system using 2 M MEA to capture CO_2 from a flue gas containing 15% CO_2/80% N_2/5% O_2 and performing electrolysis of the CO_2-capturing MEA at 50 mA·cm^{-2} for 24 h: (B) concentration of CO_2 leaving the concerted system ($[CO_2]_{outlet}$); (C) FE for CO and H_2; (D) cumulative volume of gaseous products; (E) CO_2 capture efficiency. The shaded region in Figure 3B shows the CO_2 concentration change in the outlet gas stream during 12 h CO_2 capture from a simulated flue gas (15% CO_2/80% N_2/5% O_2) using 2 M MEA. MEA: Monoethanolamine; FE: Faraday efficiencies.

approximately 12 h, the system enters a dynamic equilibrium where the CO_2 capture rate matches the electrochemical conversion rate, accomplishing concerted CO_2 capture and conversion.

To investigate the influence of reaction rate on the concerted CO_2 capture and conversion system, the electrolysis is then carried out at a higher current density of 100 mA·cm^{-2} [Supplementary Figure 13]. However, a lower FE_{CO} of 20% is observed due to the intensified HER. Nevertheless, a higher CO_2 capture efficiency of 73% is achieved compared to electrolysis at 50 mA·cm^{-2}, which can be attributed to accelerated regeneration of MEA driven by the enhanced consumption of reactive carbon species at the higher electrolysis current density. This result shows that

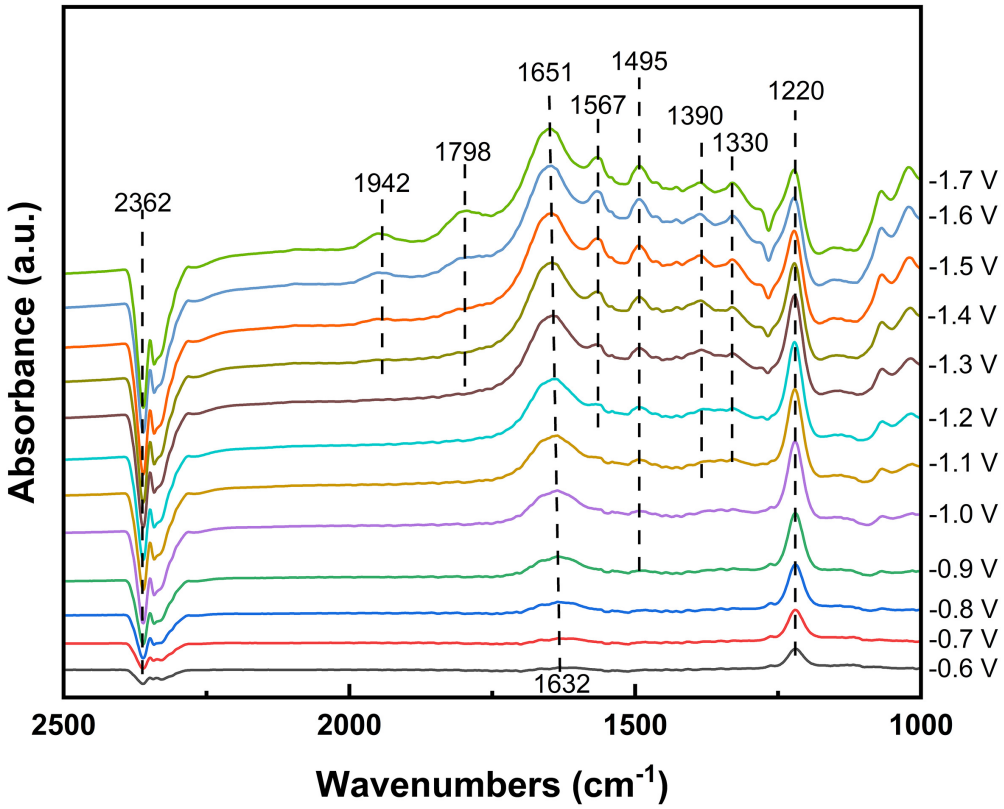

Figure 4. *In situ* ATR-FTIR spectra for electrolysis of 2 M MEA solution saturated with 15% CO_2/5% O_2/80% N_2 flue gas at varying potentials under N_2 atmosphere. ATR-FTIR: Attenuated total reflection Fourier transform infrared; MEA: monoethanolamine.

increasing the current density of electrolysis can improve CO_2 capture efficiency, though it may reduce the efficiency of the subsequent conversion step. Therefore, a trade-off exists between the efficiencies of CO_2 capture and electrochemical conversion.

To gain molecular-level insight into the electrode environment during this concerted process, we employed *in situ* ATR-FTIR spectroscopy to monitor the electrolysis of a 2 M MEA solution pre-saturated with the simulated flue gas (15% CO_2/80% N_2/5% O_2). As shown in Figure 4, during potentiostatic electrolysis, a distinct decrease in the CO_2 characteristic peak (2,362 cm^{-1}) was observed, indicating CO_2 consumption at the electrode surface[52,53]. Key solution species were identified by peaks at 1,567, 1,495, 1,390, and 1,330 cm^{-1}, which were attributed to $RNHCOO^-$[53]. The peak at 1,222 cm^{-1} corresponded to HCO_3^-[54], consistent with the NMR results [Supplementary Figure 2]. The presence of MEA-H^+ (1,632-1,651 cm^{-1}) was also confirmed, though this peak may overlap with water bending vibrations in the same range[52,55]. Notably, weak features associated with adsorbed CO intermediates (CO_L at ~1,944 cm^{-1} and CO_B at ~1,795 cm^{-1}) were detected, offering insight into the surface reaction pathway on the Ni-N-C catalyst[56]. This *in situ* analysis supports the proposed mechanism, where H^+ from the BPM facilitates MEA regeneration and the release of CO_2 from carbamate/bicarbonate pools, which is then reduced to CO at the Ni-N-C working electrode.

Building on this understanding of the electrode microenvironment, we sought to further enhance the CO_2 conversion efficiency by modifying the electrode structure. We incorporated PTFE into the Ni-N-C catalyst to increase the hydrophobicity of the electrode surface, a feature that has been shown to suppress HER[57]. Using the same procedure as for the Ni-N-C electrode, 100 μL of 2 wt% PTFE solution was added to the catalyst ink to fabricate the Ni-N-C-PTFE electrode. CO_2 capture and electrolysis were then carried out simultaneously by applying a constant current of 50 mA·cm^{-2} in 15% CO_2-capturing MEA solution [Figure 5 and Supplementary Fig-

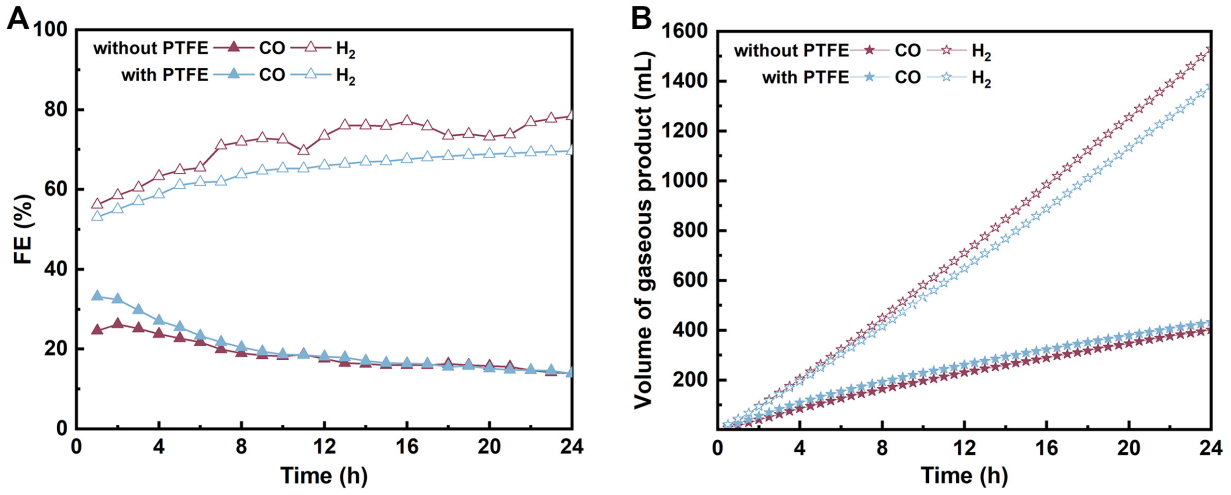

Figure 5. (A) FE and (B) cumulative volume of CO and H_2 produced in the concerted CO_2 capture and conversion system using 2 M MEA as the capture medium and conducting electrolysis at 50 mA·cm^{-2} under 15% CO_2/80% N_2/5% O_2 with Ni-N-C and Ni-N-C-PTFE electrodes. FE: Faraday efficiencies; MEA: monoethanolamine; PTFE: polytetrafluoroethylene.

ure 14]. As shown in Figure 5A, the Ni-N-C-PTFE electrode exhibits a FE_{CO} of up to 32% within the first 2 h, surpassing the unmodified Ni-N-C electrode (FE_{CO} = 26%). Over the following 22 h, however, the FE_{CO} gradually declines, eventually reaching the same level in both cases. The corresponding CO_2 capture efficiency remains stable at ~63%, consistent with that observed for the unmodified Ni-N-C cathode [Supplementary Figure 14B]. Encouragingly, the higher initial CO production rate with the PTFE-modified electrode results in a cumulative output of 432 mL CO and 1,381 mL H_2, forming a syngas with a H_2/CO = 3.2, lower than 3.8 for the unmodified electrode. The resulting syngas composition is suitable for Fischer-Tropsch synthesis to produce value-added liquid fuels, such as light olefins[58].

We also performed electrolysis of 15% CO_2-capturing MEA under a N_2 flow to examine the role of continuous CO_2 supply. At the same current density (50 mA·cm^{-2}), the $[CO_2]_{outlet}$ is lower in the absence of CO_2 feed than with the supply of 15% CO_2 [Supplementary Figure 15A]. Consequently, FE_{CO} remains lower under N_2 flow than under 15% CO_2 throughout the 24 h of electrolysis. Notably, FE_{CO} declines to only 5% at the end of 24 h of electrolysis under N_2 flow [Supplementary Figure 15B]. As a result, 269 mL CO and 1,685 mL H_2 are produced with a H_2/CO = 6.3 [Supplementary Figure 15C]. Additionally, the solution pH rises from 8.3 to 9.3 [Supplementary Figure 15D], compared with only a slight increase to 8.6 under 15% CO_2/80% N_2/5% O_2 supply. This is primarily because MEA regenerated during electrolysis cannot recapture CO_2 and therefore accumulates in the absence of CO_2 feeding. The marked differences between electrolysis experiments using flue gas and N_2 streams confirm that considerable CO is produced directly through the capture and electrochemical conversion of CO_2 in flue gas.

Since the composition of flue gas varies in real-world scenarios, we then examine the influence of CO_2 concentration in simulated flue gas on the efficiency of CO_2 capture and subsequent conversion. To this end, the CO_2 concentration is varied from 15% to 5% by diluting with N_2 and O_2. The resulting gas mixtures are continuously bubbled into 2 M MEA solutions at the same flow rate (50 sccm) to perform CO_2 capture. Due to the lower CO_2 concentration, CO_2 capture requires an additional 10 h for flue gas containing 5% CO_2 compared with its 15% CO_2 counterpart, as evidenced by measurements of the CO_2 concentration in the outlet gas and the pH of the MEA solution [Figure 6A and Supplementary Figure 16]. Notably, a higher steady-state pH is observed in the system supplied with 5% CO_2, suggesting that a lower CO_2 partial pressure reduces CO_2 loading at the end of CO_2 capture.

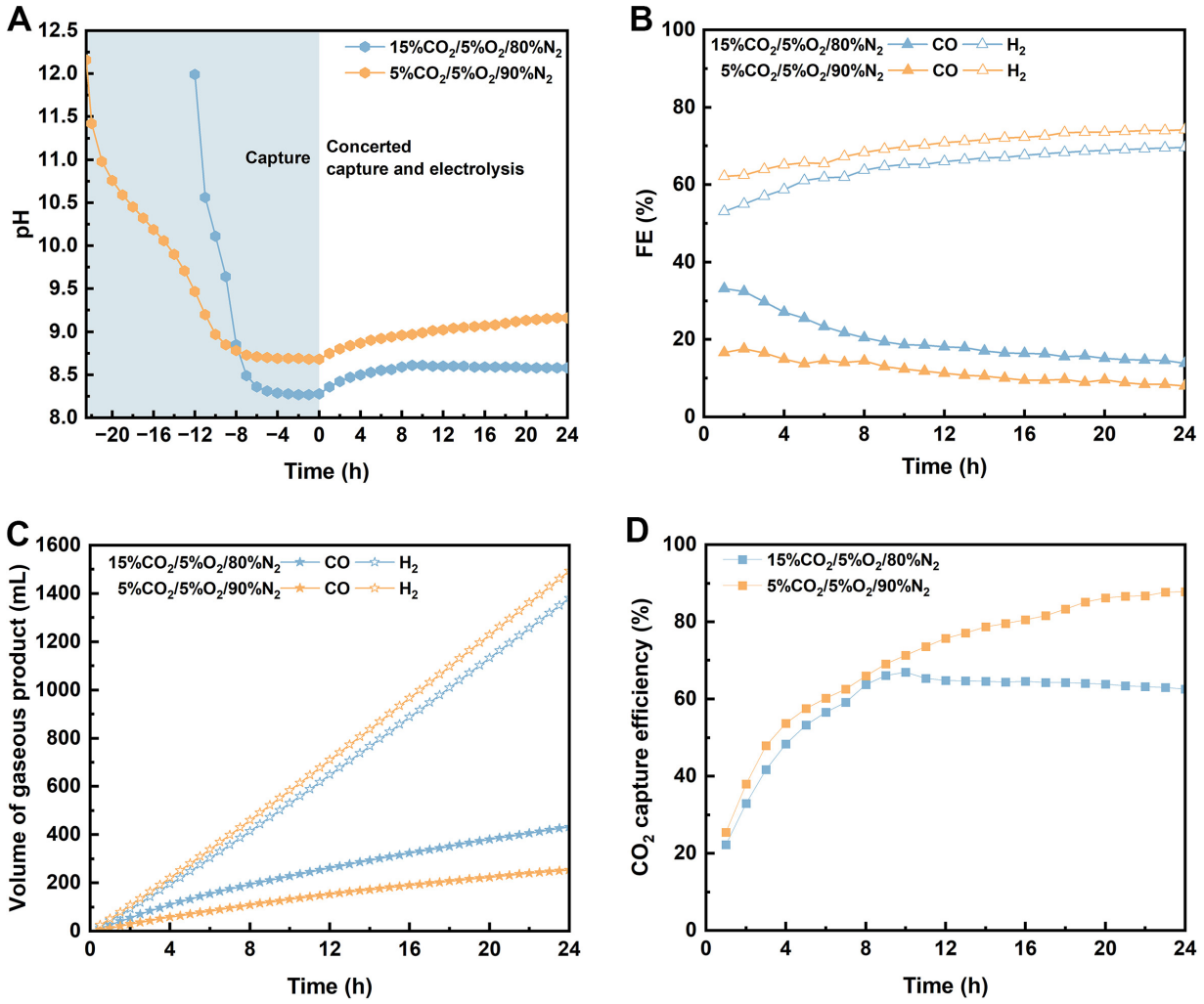

Figure 6. Efficiency of concerted CO_2 capture and conversion system using 2 M MEA to capture CO_2 from a flue gas containing 15% CO_2/5% O_2/80% N_2 or 5% CO_2/5% O_2/90% N_2 and conducting electrolysis of the CO_2-capturing MEA at 50 mA·cm^{-2} for 24 h: (A) pH evolution during CO_2 capture and subsequent conversion; (B) FE for CO and H_2 production; (C) cumulative volume of CO and H_2 products; (D) CO_2 capture efficiency. The shaded region in Figure 6A shows the pH change in the solution during 12 and 24 h CO_2 capture from simulated flue gases (15% CO_2/80% N_2/5% O_2 and 5% CO_2/90% N_2/5% O_2) using 2 M MEA. MEA: Monoethanolamine.

Similarly, concerted capture and electrochemical conversion of CO_2 from flue gas containing 5% CO_2 are performed using the Ni-N-C-PTFE electrode under the same conditions used for flue gas containing 15% CO_2. As shown in Figure 6B and C, the FE_{CO} recorded in 5% CO_2-capturing MEA solution is consistently lower than that in a 15% CO_2-capturing MEA solution, resulting in the production of 254 mL CO and 1,495 mL H_2. This decrease in FE_{CO} can be attributed to the reduced partial pressure of CO_2, which lowers the CO_2 loading in MEA and thus reduces the concentration of reactive carbon species available for electrochemical conversion. Nonetheless, the full-cell voltages recorded in 5% CO_2 and 15% CO_2-capturing MEA solutions are comparable, despite marked differences in CO_2 loading and product distribution [Supplementary Figure 17]. This is due to the increased HER activity at lower CO_2 concentrations. Notably, the CO_2 capture efficiency increases from 67% when supplied with 15% CO_2 flue gas to 88% when supplied with 5% CO_2 flue gas [Figure 6D]. Additionally, for both CO_2 concentrations, the solution pH increases during electrolysis as a result of MEA regeneration associated with CO_2 conversion and HER [Figure 6A]. The rate of pH increase in the system with 5% CO_2 is faster than that with 15% CO_2, because the CO_2 capture rate is lower than the MEA regeneration rate under low-concentration CO_2.

Building on the above parameter optimization, we determined that CO_2 capture from 15% CO_2 by 2 M MEA and electrolysis at 50 mA·cm^{-2} with the Ni-N-C-PTFE electrode provides a favorable balance between CO_2 capture efficiency and CO selectivity. To further elucidate the origin of this balance, we analyze the dynamic relationship between CO_2 capture and electrolysis by calculating CO_2 capture rate and CO production rate (the latter corresponding to the MEA regeneration rate), enabling a quantitative evaluation of their relationship during operation.

The reactions involved in CO_2 capture and electrolysis processes are presented in Supplementary Equations 1-14 in Supplementary Figure 18. As shown in Supplementary Figure 19, the CO_2 capture rate is very low initially. This is because the starting solution is a 15% CO_2-capturing MEA solution, in which MEA predominantly exists as MEA-H$^+$, carbamate, and HCO_3^- [Supplementary Equations 1-3], leaving negligible free MEA available for additional CO_2 absorption. Upon electrolysis, several steps occur simultaneously. Water splitting occurs at the BPM of the membrane electrode assembly, generating H$^+$ and OH$^-$ [Supplementary Equation 4]. In an ideal case, all H$^+$ react with carbamate and bicarbonate species to release CO_2 and partially regenerate MEA [Supplementary Equations 5 and 6]. The CO_2 is then reduced to CO at the cathode, generating CO and OH$^-$ [Supplementary Equation 7]. The OH$^-$ can react with MEA-H$^+$ [Supplementary Equation 8], regenerating MEA completely. At the anode, the OH$^-$ from water splitting is oxidized to generate O_2 [Supplementary Equation 12]. Overall, the net reaction for CO_2 capture and conversion is CO_2 splitting [Supplementary Equation 13], which simultaneously depletes the captured CO_2 species and regenerates MEA [Supplementary Equations 5-8]. However, the electrolysis system is very complicated. Some H$^+$ from the BPM and MEA-H$^+$ itself will be reduced directly to generate H_2 [Supplementary Equations 10 and 11], competing with CO_2 release and reduction steps. However, the overall reaction for H_2 evolution will not regenerate MEA [Supplementary Equation 14]. In addition, some H$^+$ will react with OH$^-$ generated during CO_2 reduction, neutralizing the additionally generated OH$^-$ in the cathodic chamber [Supplementary Equation 9]. Therefore, the MEA regeneration rate would in principle be the same as the CO production rate.

As the concentration of free MEA increases, the solution progressively regains its capacity to capture CO_2, leading to a continuous increase in the CO_2 capture rate. Around 12 h, a dynamic balance between MEA regeneration by electrolysis and consumption by CO_2 capture is established, and the capture rate approaches a steady state [Supplementary Figure 19].

In contrast, the CO production rate gradually decreases over time. This decline is primarily attributed to the increase in local pH near the cathode. Continuous CO_2 reduction generates OH$^-$ [Supplementary Equation 7], which raises the electrode interfacial alkalinity and shifts the equilibrium away from free CO_2 (toward carbonate/bicarbonate species). This shift makes CO_2 release more difficult, thereby reducing the availability of molecular CO_2 for electroreduction. In addition, prolonged operation may also induce catalyst surface changes and mass transport limitations, further contributing to the decrease in CO production rate.

Notably, the CO_2 capture rate and CO production rate intersect at approximately 4.5 h [Supplementary Figure 19]. This crossover point represents a transient state where CO_2 supply and consumption are momentarily balanced. However, due to the direct reduction of H$^+$ from BPM [Supplementary Equation 10], the generated OH$^-$ from CO_2 reduction cannot be immediately neutralized [Supplementary Equation 9], which can capture additional CO_2. This indicates that the capture capacity of the catholyte has not yet been reached. As a result, the capture rate continues to rise beyond this point, while the CO production rate cannot be sustained due to the progressively unfavorable cathodic microenvironment. At a certain point (under the selected CO_2 capture and electrolysis conditions for ~12 h), the balance for CO_2 capture and electrolysis is reached.

These results demonstrate that the rate mismatch originates from the different temporal evolution of CO_2 capture in the bulk solution versus CO_2 conversion at the electrode. Importantly, this balance can

be tuned by adjusting both CO_2 supply (inlet CO_2 concentration) and CO_2 utilization (electrolysis current density), enabling optimal conditions under which CO_2 capture efficiency and CO selectivity are simultaneously optimized.

Finally, the MEA-mediated concerted system is compared with both conventional sequential and recently reported carbonate-based concerted systems [Supplementary Table 1]. The comparison involves key metrics such as Faraday efficiency and partial current density for CO production, total current density, stability, CO_2 capture efficiency, and energy consumption (Details of the energy consumption calculation are provided in Supplementary Note 1). We note that the Faraday efficiency and partial current density for CO production of our MEA-mediated system are currently lower than those of conventional sequential systems, yet comparable to recently reported carbonate-based concerted systems. Notably, our system offers an advantage in overall energy consumption compared to the conventional sequential route, as it eliminates the need for energy-intensive upstream CO_2 desorption (e.g., thermal regeneration). Additionally, our system also exhibits a twofold higher CO_2 capture efficiency compared to carbonate-based concerted systems, because of the faster CO_2 absorption kinetics of amines. These results suggest that the MEA-mediated system enables effective CO_2 capture and utilization.

CONCLUSIONS

We have developed an MEA-based system for concerted CO_2 capture and electrochemical conversion by combining a simple CO_2 absorber with a liquid-fed electrolyzer. The CO_2-capturing MEA solution is directly utilized as the liquid feedstock for electrochemical conversion, enabling *in situ* CO_2 release and subsequent syngas production over a Ni single-atom catalyst. The system shows strong tolerance to oxygen and is feasible for concerted CO_2 capture and electrochemical conversion under flue gas conditions. Through optimization of current density, electrode hydrophobicity, and CO_2 concentration, we achieved a high CO_2 capture efficiency of 63% and efficiently produce syngas with H_2/CO = 3.2. This work demonstrates the feasibility of MEA-mediated concerted CO_2 capture-conversion for flue gas upgrading, while further optimizations in amine structure, catalyst stability, electrode design, and system operation are warranted for long-term applications.

DECLARATIONS

Authors' contributions

Performed research and analyzed data: Yin, C. Q.
Assisted with the electrolysis and data analysis: Zou, Y. B.; Lv, Z. H.
Conceived and supervised the research: Li, Y.; Hu, X. M.
Wrote and revised the manuscript: Yin, C. Q.; Du, L.; Li, Y.; Hu, X. M.

Availability of data and materials

The data that support the findings of this study are available from the corresponding author upon reasonable request.

AI and AI-assisted tools statement

Not applicable.

Financial support and sponsorship

This work was financially supported by National Natural Science Foundation of China (Nos. 22509114, and 22376120), Taishan Scholars program from Shandong Province (Nos. tsqn202103021, and tsqn202507032), and Shandong Provincial Natural Science Foundation (No. ZR2025QC1317).

Conflicts of interest

All authors declared that there are no conflicts of interest.

Ethical approval and consent to participate

Not applicable.

Consent for publication

Not applicable.

Supplementary Materials

Supplementary Materials

REFERENCES

1. Babila, T. L.; Penman, D. E.; Standish, C. D.; et al. Surface ocean warming and acidification driven by rapid carbon release precedes Paleocene-Eocene Thermal Maximum. *Sci. Adv.* **2022**, *8*, eabg1025. DOI PubMed PMC

2. Huang, M.; Reich, P. B.; Wang, S.; et al. Nitrogen and CO_2 enrichment interact to decrease biodiversity impact on complementarity and selection effects. *Nat. Commun.* **2025**, *16*, 7445. DOI PubMed PMC
3. Garg, S.; Biswas, A. N.; Chen, J. G. Opportunities for CO_2 upgrading to C_3 oxygenates using tandem electrocatalytic-thermocatalytic processes. *Carbon. Future.* **2024**, *1*, 9200002. DOI
4. Allangawi, A.; Xiao, X. T.; Ma, X.; et al. Selective electrocatalytic CO_2 reduction to methanol: a roadmap toward practical implementation. *Angew. Chem. Int. Ed.* **2025**, *64*, e202517916. DOI PubMed
5. Zou, J.; Gupta, D.; Liang, G. CO_2 utilization in energy storage and conversion. *J. Mater. Chem. A.* **2025**, *13*, 32004-29. DOI
6. Chen, C.; Kosari, M.; Jiang, Z.; et al. Boosting CO_2 hydrogenation to methanol via enriching the Cu–ZnO interface on layered double oxides. *Small* **2025**, *21*, 2412786. DOI PubMed
7. De La Torre, P.; An, L.; Chang, C. J. Porosity as a design element for developing catalytic molecular materials for electrochemical and photochemical carbon dioxide reduction. *Adv. Mater.* **2023**, *35*, 2302122. DOI PubMed
8. Patil, O. U.; Park, S. Recent progress of the electrocatalytic CO_2 reduction reaction using porous materials. *Chem. Commun.* **2025**, *61*, 9531-42. DOI PubMed
9. Nzotcha, U.; Sanz, S.; Tempel, H.; Eichel, R. A. Technoeconomic perspective on the electroreduction of CO_2 to formic acid: scale-up strategies toward industrial viability. *Angew. Chem. Int. Ed.* **2025**, *64*, e202418114. DOI PubMed
10. Sun, Q.; Jia, C.; Lu, H.; et al. Ampere-level electroreduction of CO_2 and CO. *Chem. Soc. Rev.* **2025**, *54*, 6973-7016. DOI PubMed
11. Pimlott, D. J. D.; Jewlal, A.; Kim, Y.; Berlinguette, C. P. Oxygen-resistant CO_2 reduction enabled by electrolysis of liquid feedstocks. *J. Am. Chem. Soc.* **2023**, *145*, 25933-7. DOI PubMed
12. Harvey, C. M.; Chardon-noblat, S.; Costentin, C. Self-protection mechanism and mass transport governing O_2 tolerance in an iron porphyrin homogeneous catalyst for CO_2 electroreduction. *J. Am. Chem. Soc.* **2025**, *147*, 24171-8. DOI PubMed
13. Cheng, Y.; Hou, P.; Wang, X.; Kang, P. CO_2 electrolysis system under industrially relevant conditions. *Acc. Chem. Res.* **2022**, *55*, 231-40. DOI PubMed
14. Xie, L.; Cai, Y.; Jiang, Y.; et al. Direct low concentration CO_2 electroreduction to multicarbon products via rate-determining step tuning. *Nat. Commun.* **2024**, *15*, 10386. DOI PubMed PMC
15. Gao, W.; Liang, S.; Wang, R.; et al. Industrial carbon dioxide capture and utilization: state of the art and future challenges. *Chem. Soc. Rev.* **2020**, *49*, 8584-686. DOI PubMed
16. Zhang, S.; Tang, W.; Yin, J.; et al. Feasibility and prospects of electrocatalytic conversion of CO_2 for chemical feedstock production and renewable energy storage. *ACS. Sustainable. Chem. Eng.* **2025**, *13*, 9841-58. DOI
17. Elgazzar, A.; Zhu, P.; Chen, F.; et al. Electrochemical CO_2 reduction to formic acid with high carbon efficiency. *ACS. Energy. Lett.* **2024**, *10*, 450-8. DOI
18. Belsa, B.; Xia, L.; García De Arquer, F. P. CO_2 electrolysis technologies: bridging the gap toward scale-up and commercialization. *ACS. Energy. Lett.* **2024**, *9*, 4293-305. DOI PubMed PMC
19. Osorio-tejada, J.; Escriba-gelonch, M.; Vertongen, R.; Bogaerts, A.; Hessel, V. CO_2 conversion to CO *via* plasma and electrolysis: a techno-economic and energy cost analysis. *Energy. Environ. Sci.* **2024**, *17*, 5833-53. DOI PubMed PMC
20. Deng, W.; Lee, A.; Dai, W.; et al. Techno-economics of polymer-membrane-based CO_2 electrolysers. *Nat. Rev. Clean. Technol.* **2025**, *1*, 255-68. DOI
21. Yulia, F.; Sofianita, R.; Prayogo, K.; Nasruddin, N. Optimization of post combustion CO_2 absorption system monoethanolamine (MEA) based for 320 MW coal-fired power plant application - exergy and exergoenvironmental analysis. *Case. Stud. Therm. Eng.* **2021**, *26*, 101093. DOI
22. Fytianos, G.; Grimstvedt, A.; Knuutila, H.; Svendsen, H. F. Effect of MEA's degradation products on corrosion at CO_2 capture plants. *Energy. Procedia.* **2014**, *63*, 1869-75. DOI
23. Vevelstad, S. J.; Buvik, V.; Knuutila, H. K.; Grimstvedt, A.; Da Silva, E. F. Important aspects regarding the chemical stability of aqueous amine solvents for CO_2 capture. *Ind. Eng. Chem. Res.* **2022**, *61*, 15737-53. DOI
24. Namdari, M.; Kim, Y.; Pimlott, D. J. D.; Jewlal, A. M. L.; Berlinguette, C. P. Reactive carbon capture using electrochemical reactors. *Chem. Soc. Rev.* **2025**, *54*, 590-600. DOI PubMed
25. Zhang, Z.; Lees, E. W.; Habibzadeh, F.; et al. Porous metal electrodes enable efficient electrolysis of carbon capture solutions. *Energy. Environ. Sci.* **2022**, *15*, 705-13. DOI
26. Song, H.; Fernández, C. A.; Choi, H.; Huang, P.; Oh, J.; Hatzell, M. C. Integrated carbon capture and CO production from bicarbonates through bipolar membrane electrolysis. *Energy. Environ. Sci.* **2024**, *17*, 3570-9. DOI
27. Leverick, G.; Bernhardt, E. M.; Ismail, A. I.; et al. Uncovering the active species in amine-mediated CO_2 reduction to CO on Ag. *ACS. Catal.* **2023**, *13*, 12322-37. DOI
28. Zou, Y.; Zheng, A.; Feng, L.; Du, L.; Daasbjerg, K.; Hu, X. Integrated capture and electrochemical conversion of CO_2 from flue gas mediated by carbonate/bicarbonate cycle. *J. Mater. Chem. A.* **2025**, *13*, 36191-201. DOI
29. Pimlott, D. J. D.; Kim, Y.; Berlinguette, C. P. Reactive carbon capture enables CO_2 electrolysis with liquid feedstocks. *Acc. Chem. Res.* **2024**, *57*, 1007-18. DOI PubMed

30. Jewlal, A. M. L.; Kim, Y.; Crescenzo, G. V.; Berlinguette, C. P. Go with CO: a case for targeting carbon monoxide as a reactive carbon capture product. *ACS. Energy. Lett.* **2025**, *10*, 2498-502. DOI
31. Kim, Y.; Lees, E. W.; Donde, C.; et al. Integrated CO_2 capture and conversion to form syngas. *Joule* **2024**, *8*, 3106-25. DOI
32. Cai, T.; Johnson, J. K.; Wu, Y.; Chen, X. Toward understanding the kinetics of CO_2 capture on sodium carbonate. *ACS. Appl. Mater. Interfaces.* **2019**, *11*, 9033-41. DOI PubMed
33. Wang, T.; Yu, W.; Fang, M.; et al. Wetted-wall column study on CO_2 absorption kinetics enhancement by additive of nanoparticles. *Greenhouse. Gases. Sci. Technol.* **2015**, *5*, 682-94. DOI
34. Krótki, A.; Więcław Solny, L.; Stec, M.; et al. Experimental results of advanced technological modifications for a CO_2 capture process using amine scrubbing. *Int. J. Greenh. Gas. Con.* **2020**, *96*, 103014. DOI
35. Feng, L.; Lv, Z.; Kong, Y.; Hu, X. Upcycling of plastic waste to atomic nickel site-decorated carbon for efficient electrochemical CO_2 conversion. *Sustain. Energy. Fuels.* **2024**, *8*, 2860-8. DOI
36. Li, Y. C.; Lee, G.; Yuan, T.; et al. CO_2 electroreduction from carbonate electrolyte. *ACS. Energy. Lett.* **2019**, *4*, 1427-31. DOI
37. Mezzavilla, S.; Horch, S.; Stephens, I. E. L.; Seger, B.; Chorkendorff, I. Structure sensitivity in the electrocatalytic reduction of CO_2 with gold catalysts. *Angew. Chem. Int. Ed.* **2019**, *58*, 3774-8. DOI PubMed
38. Ko, Y. J.; Lim, C.; Jin, J.; et al. Extrinsic hydrophobicity-controlled silver nanoparticles as efficient and stable catalysts for CO_2 electrolysis. *Nat. Commun.* **2024**, *15*, 3356. DOI PubMed PMC
39. Wang, M.; Torbensen, K.; Salvatore, D.; et al. CO_2 electrochemical catalytic reduction with a highly active cobalt phthalocyanine. *Nat. Commun.* **2019**, *10*, 3602. DOI PubMed PMC
40. Wu, X.; Zhao, J. Y.; Sun, J. W.; et al. Isolation of highly reactive cobalt phthalocyanine via electrochemical activation for enhanced CO_2 reduction reaction. *Small* **2023**, *19*, 2207037. DOI PubMed
41. Karapinar, D.; Huan, N. T.; Ranjbar Sahraie, N.; et al. Electroreduction of CO_2 on single-site copper-nitrogen-doped carbon material: selective formation of ethanol and reversible restructuration of the metal sites. *Angew. Chem. Int. Ed.* **2019**, *58*, 15098-103. DOI PubMed
42. Paul, S.; Kao, Y.; Ni, L.; et al. Influence of the metal center in M-N-C catalysts on the CO_2 reduction reaction on gas diffusion electrodes. *ACS. Catal.* **2021**, *11*, 5850-64. DOI
43. Varela, A. S.; Ju, W.; Bagger, A.; Franco, P.; Rossmeisl, J.; Strasser, P. Electrochemical reduction of CO_2 on metal-nitrogen-doped carbon catalysts. *ACS. Catal.* **2019**, *9*, 7270-84. DOI
44. Li, Y.; Lu, X. F.; Xi, S.; Luan, D.; Wang, X.; Lou, X. W. Synthesis of N-doped highly graphitic carbon urchin-like hollow structures loaded with single-Ni atoms towards efficient CO_2 electroreduction. *Angew. Chem. Int. Ed.* **2022**, *61*, e202201491. DOI PubMed
45. Wang, J.; Huang, Y.; Wang, Y.; et al. Atomically dispersed metal-nitrogen-carbon catalysts with *d*-orbital electronic configuration-dependent selectivity for electrochemical CO_2-to-CO reduction. *ACS. Catal.* **2023**, *13*, 2374-85. DOI
46. Wang, H.; Liu, G.; Chen, C.; et al. Single-Ni sites embedded in multilayer nitrogen-doped graphene derived from amino-functionalized MOF for highly selective CO_2 electroreduction. *ACS. Sustainable. Chem. Eng.* **2021**, *9*, 3792-801. DOI
47. Wattanaphan, P.; Sema, T.; Idem, R.; Liang, Z.; Tontiwachwuthikul, P. Effects of flue gas composition on carbon steel (1020) corrosion in MEA-based CO_2 capture process. *Int. J. Greenh. Gas. Con.* **2013**, *19*, 340-9. DOI
48. Xu, Y.; Edwards, J. P.; Zhong, J.; et al. Oxygen-tolerant electroproduction of C_2 products from simulated flue gas. *Energy. Environ. Sci.* **2020**, *13*, 554-61. DOI
49. Li, P.; Lu, X.; Wu, Z.; et al. Acid-base interaction enhancing oxygen tolerance in electrocatalytic carbon dioxide reduction. *Angew. Chem. Int. Ed. Engl.* **2020**, *59*, 10918-23. DOI PubMed
50. Weiss, R. Carbon dioxide in water and seawater: the solubility of a non-ideal gas. *Mar. Chem.* **1974**, *2*, 203-15. DOI
51. Wei, X, Yin, G., Zhang, J., Eds. *Rotating Electrode Methods and Oxygen Reduction Electrocatalysts*; Elsevier, 2014. DOI
52. Bruggeman, D. F.; Rothenberg, G.; Garcia, A. C. Investigating proton shuttling and electrochemical mechanisms of amines in integrated CO_2 capture and utilization. *Nat. Commun.* **2024**, *15*, 9207. DOI PubMed PMC
53. Li, P.; Mao, Y.; Shin, H.; et al. Tandem amine scrubbing and CO_2 electrolysis via direct piperazine carbamate reduction. *Nat. Energy.* **2025**, *10*, 1262-73. DOI
54. Coenen, K.; Gallucci, F.; Mezari, B.; Hensen, E.; Van Sint Annaland, M. An *in-situ* IR study on the adsorption of CO_2 and H_2O on hydrotalcites. *J. CO2. Util.* **2018**, *24*, 228-39. DOI
55. Mei, Z.; He, Y.; Liu, K.; et al. Enhanced *COOH adsorption over edge-rich Ni–N_4 sites for efficient acidic CO_2 electroreduction. *J. Am. Chem. Soc.* **2025**, *147*, 34101-8. DOI PubMed
56. Dunwell, M.; Yan, Y.; Xu, B. *In situ* infrared spectroscopic investigations of pyridine-mediated CO_2 reduction on Pt electrocatalysts. *ACS. Catal.* **2017**, *7*, 5410-9. DOI

57. Liang, H.; Zhao, S.; Hu, X.; Ceccato, M.; Skrydstrup, T.; Daasbjerg, K. Hydrophobic copper interfaces boost electroreduction of carbon dioxide to ethylene in water. *ACS. Catal.* **2021**, *11*, 958-66. DOI

58. Jiao, F.; Li, J.; Pan, X.; et al. Selective conversion of syngas to light olefins. *Science* **2016**, *351*, 1065-8. DOI PubMed